NATIONAL TRANSPORTATION SAFETY BOARD
Office of Aviation Safety

STRUCTURES GROUP CHAIRMAN'S RUDDER LOADS STUDY

September 9, 2021

A. ACCIDENT ANC20LA059

Operator:	Private
Location:	Anchorage, Alaska
Date:	June 8, 2020
Time:	0945 Alaska Daylight Time (ADT)
Aircraft:	Piper PA-12
Registration:	N3188M

B. STRUCTURES GROUP

Chairman:	Clinton R. Crookshanks National Transportation Safety Board Denver, Colorado
Member:	Dave Swartz Federal Aviation Administration Anchorage, Alaska
Member:	Jonathon Hirsch Piper Aircraft, Inc. Vero Beach, Florida

C. SUMMARY

On June 8, 2020, about 0945 Alaska daylight time, a float-equipped Piper PA-12 airplane, N3188M, sustained substantial damage when it's rudder structurally failed in flight about 8 miles north of Anchorage, Alaska. The flight instructor and private pilot receiving instruction were not injured. The airplane was operated as a Title 14 Code of Federal Regulations Part 91 instructional flight.

According to the flight instructor, they departed Lake Hood Airport (PALH) and proceeded to Twin Island Lake (about 8 nm northwest of PALH), where upon arrival, they conducted a

normal landing. After departing, they climbed to about 500 ft above ground level (agl) before turning to a left crosswind traffic pattern leg. While on the left crosswind leg, the airplane yawed abruptly to the right and the private pilot indicated that the controls felt strange. The flight instructor assumed control of the airplane and noticed drastically diminished control about the vertical axis. In addition, significant downward elevator pressure (forward control yoke) was required. In an effort to aid in directional control the water rudders were deployed. Uncertain that he could make a 180° turn and return to Twin Island Lake due to the poor directional control, he elected to return to PALH where emergency services were available and conducted an uneventful landing.

D. DETAILS OF THE INVESTIGATION

1.0 Aircraft Examination

The NTSB did not travel to the scene or examine the aircraft in person. A representative from the Federal Aviation Administration (FAA) Anchorage Aircraft Certification Office (ACO) examined the accident airplane.

The accident airplane was equipped with a 160 HP[1] Lycoming O-320 engine and a McCauley propeller. The airplane had EDO 2000 floats installed per an STC. The rudder post was fractured at the upper end of the upper hinge barrel and the top of the rudder was folded over to the left. There was a Whelen Model 9052051 LED strobe light installed at the top of the rudder post. The data tag on the strobe light indicated it weighed 0.65 lb. A LED tail navigation light/strobe was also installed on the rudder trailing edge in place of the original navigation light.

The FAA ACO representative obtained two additional fractured rudders similar to the accident rudder from a repair station.

Figure 1-PA-12 fractured rudders; grey rudder is from accident airplane.

[1] The PA-12 airplane was originally certified and delivered with a 100 HP or 115 HP Lycoming O-235 engine.

Available information indicated that the white painted rudder came off a wheel equipped PA-12 airplane with a 180 HP Lycoming O-360 engine and the cream painted rudder came off a wheel/ski equipped PA-12 airplane with a 150 HP Lycoming O-320 engine. The white painted rudder post was fractured about ½ inch above the upper edge of the upper hinge barrel and the top of the rudder was folded over to the left. There was evidence of a light being installed at the top of the rudder post, but it wasn't installed when received. The cream painted rudder post was fractured about 1 inch above the upper edge of the upper hinge barrel and the top of the rudder was folded over to the right. There was evidence of a light being installed at the top of the rudder post, but it wasn't installed when received.

The three failed rudders were sent to the NTSB Materials Laboratory for examination. The NTSB Materials Laboratory Factual Report 20-049 for the 3 rudders can be found in the public docket for this accident.

The FAA issued an Airworthiness Concern Sheet in September 2020 for several single engine Piper airplane models detailing the circumstances of this accident and requesting information from any operators experiencing similar failures. In January 2021, the FAA received information about a rudder that was found with a fractured rudder post during inspection, Figure 2. The rudder was installed on a 1969 Piper PA-18 airplane with a 160 HP[2] Lycoming O-320 engine. The airplane had a Whelan strobe light (PN 01-0770509-02) installed at the top of the rudder post. There was no indication in the logbook that the rudder was ever replaced. The rudder was last re-covered with Ceconite 102 in 1992. A section of the rudder post containing the fracture was cut from the rudder and sent to the NTSB Materials Laboratory for examination. The rudder post was fractured about 1.3 inches above the upper edge of the upper hinge barrel. The NTSB Materials Laboratory Factual Report 21-034 can be found in the public docket for this accident.

Figure 2-PA-18 fractured rudder post.

[2] The PA-18 airplane was originally certified and delivered with a 90 HP Continental C-90, a 125 HP Lycoming O-290, a 135 HP Lycoming O-290, or a 150 HP Lycoming O-320 engine.

2.0 Rudder Information

There were no visible part numbers or other identifying markings on any of the rudders, but examination of the configuration of each indicated they were consistent with Piper P/N 40622 rudder assemblies. The NTSB Materials Laboratory determined that all four rudder posts had material compositions consistent with AISI 1025 carbon steel. According to engineering drawings, the rudder post for the P/N 40622 rudder was originally manufactured from 7/8-inch diameter, 0.035-inch wall thickness AISI 1025 carbon steel tube. In a Piper engineering change order (ECO) dated June 3, 1974, the specified material for the rudder post was changed to normalized AISI 4130 low-alloy steel with the same dimensions. The material change to 4130N was incorporated into the P/N 40622 engineering drawing at Revision U in June 1974. The P/N 40622 rudder can be installed on PA-12 and PA-18 airplanes and some other single engine Piper airplanes.

The P/N 40622 rudder was drawn in AutoCAD to aid in calculating the total area and centroid for each of the failed rudders. The trailing edge navigation light housing and the upper beacon light housing were not included on the drawing. Per the NTSB lab report, the accident airplane (N3188M) grey rudder was identified as Rudder A, the white rudder was identified as Rudder B, and the cream rudder was identified as Rudder C. The yellow rudder submitted later was identified as Rudder D. The failed sections of each rudder were also drawn in AutoCAD with the centroid location and area as shown in Appendix A.

The Rudder A area was calculated to be 313.41 in^2 and the centroid was located 9-1/16 inches below the top of the rudder and 7/16 inch aft of the rudder post centerline. The Rudder B area was calculated to be 305.75 in^2 and the centroid was located 8-7/8 inches below the top of the rudder and 5/16 inch aft of the rudder post centerline. The Rudder C area was calculated to be 298.19 in^2 and the centroid was located 8-11/16 inches below the top of the rudder and 1/8 inch aft of the rudder post centerline. The Rudder D area was calculated to be 293.72 in^2 and the centroid was located 8-9/16 inches below the top of the rudder and on the rudder post centerline.

3.0 Material Information

Piper supplied a copy of the ANC-5 Bulletin, *Strength of Metal Aircraft Elements*, published in 1951 by the Munitions Board Aircraft Committee as the document used during the design of the PA-12 airplane for material properties. The ANC-5 was the basis for both military and civil aircraft design and was acceptable for use by the Navy, Air Force, and Civil Aeronautics Authority. ANC-5, Chapter 2, Steel, contained the material properties for AISI 1025 and AISI 4130N steel as follows.

AISI 1025 Steel Tubing	AISI 4130N Steel Tubing
F_{tu} = 55 ksi	F_{tu} = 90 ksi
$F_{ty} = F_{cy}$ = 36 ksi	$F_{ty} = F_{cy}$ = 70 ksi

The ANC-5 bulletin eventually morphed into MIL-HDBK-5 that was maintained by the US Air Force as the repository for all aircraft material information. In the last 20 years the MIL-HNDBK was replaced by the *Metallic Materials Properties Development and Standardization (MMPDS) Handbook* maintained by the FAA William J. Hughes Technical Center. The current version, MMPDS-04, is an accepted source for metallic material and fastener system allowables for the

FAA, all Departments and Agencies of the Department of Defense (DoD), and the National Aeronautics and Space Administration (NASA).

MMPDS-04, Chapter 2, Steels, classifies AISI 1025 steel as a carbon steel since it contains carbon up to about 1%. In general, the corrosion resistance of carbon steels is relatively poor unless it is plated or has some other surface treatment. "AISI 1025 is an excellent general purpose steel for the majority of shop requirements, including jigs, fixtures, prototype mockups, low-torque shafting, and other applications. It is not generally classed as an airframe structural steel. However, it is available in aircraft quality as well as commercial quality." The values for the ultimate tensile strength (F_{tu}), tensile yield strength (F_{ty}), and compressive yield strength (F_{cy}) in MMPDS-04 are the same as quoted from ANC-5.

MMPDS-04 classifies AISI 4130N steel as a low-alloy chromium-molybdenum steel. In general, the low-alloy steels have better strength-to-weight ratios and, in some cases, somewhat better corrosion resistance than carbon steels. AISI 4130N steel is considered an airframe structural steel and is typically used for aircraft structure requiring high strength, through hardening, or toughness. The values for the ultimate tensile strength, tensile yield strength, and compressive yield strength in MMPDS-04 are the same as quoted from ANC-5.

The PA-12 and PA-18 airplanes were designed for static load conditions as dictated by the regulations in place at the time. However, in service, the loading conditions on many parts of the structure, including the rudder, are not static and contain dynamic alternating or repeated (fatigue) loads. It is well documented that fatigue failures in metal occur at stress levels well below the static strength stress levels. Aircraft designed in accordance with modern regulations must account for fatigue loads. As part of the modern design process, materials used for aircraft structure must have published fatigue test data in the form of stress-life (S-N) curves. An example of this data is shown in Figure 3 for unnotched AISI 4130N alloy steel sheet from MMPDS-04.

Fatigue test data for steel generally shows a flattening of the S-N curves as the number of fatigue stress cycles increases. This flattening of the curve is called the endurance limit and is defined as the stress below which a material can endure an infinite number of repeated load cycles without failure. *Elements of Metallurgy and Engineering Alloys*, Chapter 14, published by ASM International states "For a large number of steels, there is a direct correlation between tensile strength and fatigue strength; higher-tensile-strength steels have higher endurance limits. The endurance limit is normally in the range of 0.35 to 0.60 of the tensile strength. This relationship holds up to a hardness of approximately 40 HRC (~1200 MPa, or 180 ksi tensile strength), and then the scatter becomes too great to be reliable." Most information available assumes the endurance limit to be about ½ the ultimate tensile strength (F_{tu}) for those steels where F_{tu} is less than 150ksi - 200ksi.

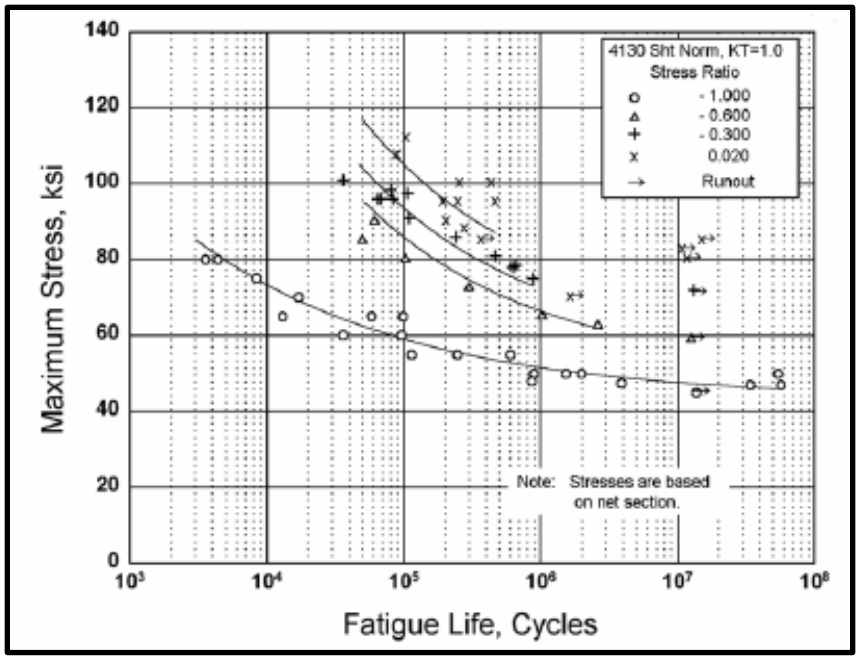

Figure 3-MMPDS-04 Figure 2.3.1.2.8(a) Best fit S-N curves for unnotched AISI 4130N sheet.

The relationship between ultimate strength and endurance limit is evident in the data of Figure 3, however, it only applies to pristine (or unnotched) material. Localized stress concentrations in the form of holes, changes in cross sectional area, notches, scratches, or corrosion will have a significant effect on the fatigue life of any material resulting in a decrease in fatigue life. In addition, standard industry practice would incorporate a scatter factor on test data such as that in Figure 3 since the data was gathered in controlled tests and is not representative of actual in-service conditions.

4.0 Aircraft Certification Information

Both the PA-12 and PA-18 airplanes were designed and certified under the Civil Air Regulations, Part 3 (CAR 3) by Piper Aircraft. The type certificate for the PA-12 and PA-12S airplanes was transferred to FS 2003 Corporation in September 2000.

The PA-12 Super Cruiser was certified in the normal and utility categories and the PA-12S was certified in the normal category per type certificate data sheet A-780. The following pertinent data will be used for the rudder load calculations later in this study.

W = 1750 lb (gross weight, landplane, normal category)
W = 1500 lb (gross weight, landplane, utility category)
W = 1838 lb (gross weight, seaplane, normal category)
S = 179.96 ft^2 (wing area)
b = 35'6" (wingspan)
c = 60 in (wing chord)
Rudder deflection = +/-20°
V_A = 94 mph (maneuvering speed)
V_C = 110 mph (cruising speed)

The average wing loading can be calculated for each of the certified weights.

W/S = 9.72 psf (landplane, normal category)
W/S = 8.34 psf (landplane, utility category)
W/S = 10.21 psf (seaplane, normal category)

The PA-18-150 Super Cub was certified in the normal and utility categories and the PA-18S-150 was certified in the normal category per type certificate data sheet 1A2. The following pertinent data will be used for rudder load calculations later in this study.

W = 1750 lb (gross weight, landplane, normal category)
W = 1500 lb (gross weight, landplane, utility category)
W = 1760 lb (gross weight, seaplane, normal category)
S = 178.5 ft^2 (wing area)
b = 35'2.5" (wingspan)
c = 60 in (wing chord)
Rudder deflection = +/-25°
V_A = 96 mph (landplane maneuvering speed)
V_A = 94 mph (seaplane maneuvering speed)
V_C = 121 mph (landplane cruising speed)
V_C = 110 (seaplane cruising speed)

The average wing loading can be calculated for each of the certified weights

W/S = 9.80 psf (landplane, normal category)
W/S = 8.40 psf (landplane, utility category)
W/S = 9.86 psf (seaplane, normal category)

5.0 Rudder Loads Calculations

The rudder post is a cantilevered beam above the upper hinge and the maximum bending stress is given by:

$$\sigma = \frac{Mc}{I} = \frac{Fyc}{I}$$

Where:

$$I = \frac{\pi}{64}(d_o^4 - d_i^4) = \frac{\pi}{64}(0.875\ in^4 - 0.805\ in^4) = 8.161x10^{-3}\ in^4$$

F = Airload acting on failed portion of rudder
y = vertical distance between the fracture location and centroid
c = radius of tube (0.4375 in)

The centroid of the failed area is assumed to be the airload application point for all calculations. There is a torsional component to the stress in the rudder post, but it is deemed to be negligible for the purposes of this study since the centroid of each failed rudder lies within 7/16" of the rudder post centerline.

The Civil Aeronautics Manual (CAM) 3 provides supplementary material, guidance, and interpretations of the regulations in CAR 3 to assist the user with regulatory compliance.

The flight maneuvering load factor n = 3.8 per CAM 3.186 for normal category airplanes and n = 4.4 for utility category airplanes.

CAM 3 provides a means for calculating the vertical tail surface maneuvering and gust loads for compliance with CAR 3.219 and 3.220, respectively. Figure 3-3(a) and 3-3(b) from CAM 3 are shown below as Figures 4 and 5.

Acceptable values of limit average maneuvering control surface loadings can be obtained from Figure 3–3 (b) as follows:

Horizontal Tail Surfaces

(1) Condition § 3.216 (a):
Obtain w as function of W/S and surface deflection;
Use Curve C for deflection 10° or less;
Use Curve B for deflection 20°;
Use Curve A for deflection 30° or more;
(Interpolate for other deflections);
Use distribution of Figure 3–8.

(2) Condition § 3.216 (b):
Obtain $\overline{w}$ from Curve B. Use distribution of Figure 3–8.

Vertical Tail Surfaces

(3) Condition § 3.219 (a):
Obtain $\overline{w}$ as function of W/S and surface deflection in same manner as outlined in (1) above, use distribution of Figure 3–8;

(4) Condition § 3.219 (b):
Obtain $\overline{w}$ from Curve C, use distribution of Figure 3–7;

(5) Condition § 3.219 (c):
Obtain $\overline{w}$ from Curve A, use distribution of Figure 3–9. (Note that condition § 3.220 generally will be more critical than this condition.)

Ailerons

(6) In lieu of conditions § 3.222 (b):
Obtain $\overline{w}$ from Curve B, acting in both up and down directions.
Use distribution of Figure 3–10.

FIG. 3-3(a)—LIMIT AVERAGE MANEUVERING CONTROL SURFACE LOADINGS

Figure 4-CAM 3 Figure 3-3(a).

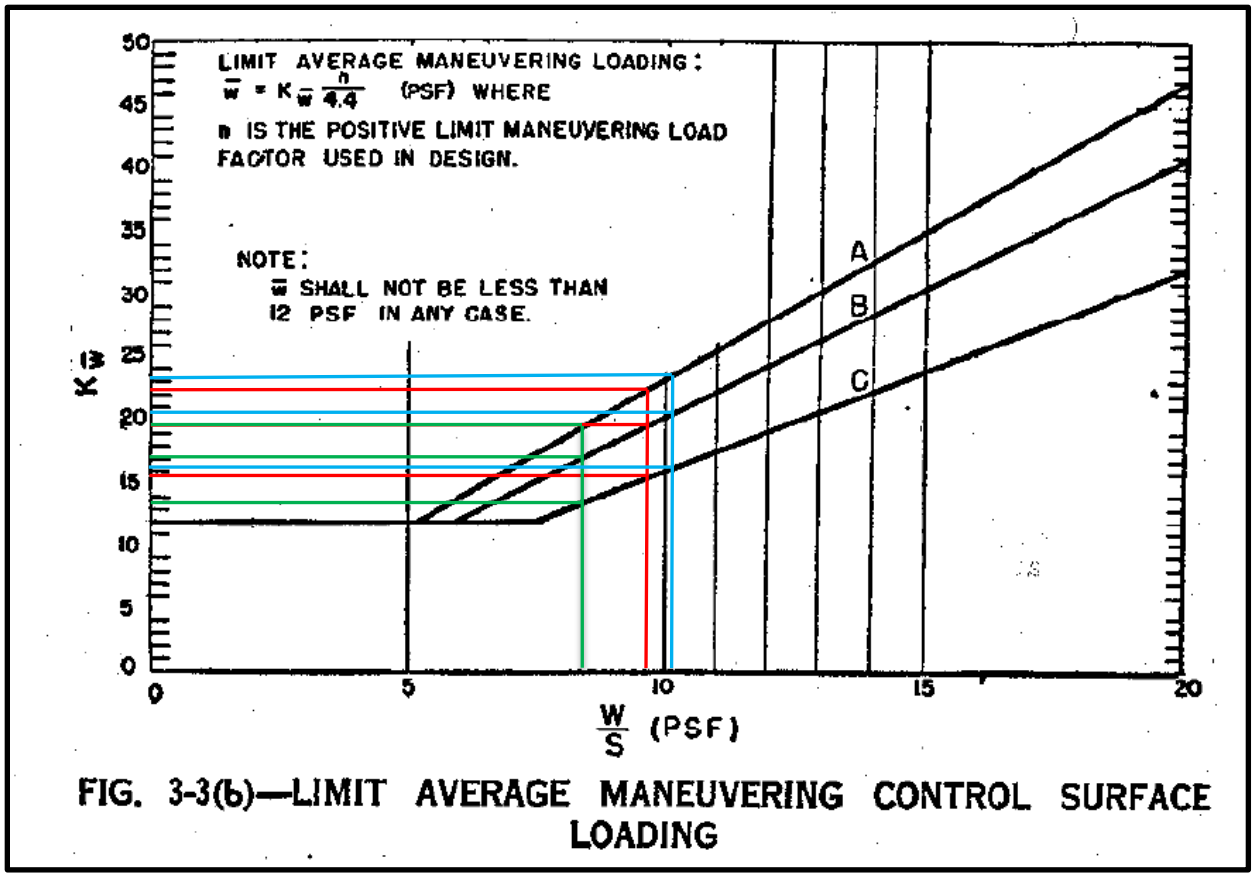

FIG. 3-3(b)—LIMIT AVERAGE MANEUVERING CONTROL SURFACE LOADING

Figure 5-CAM 3 Figure 3-3(b).

The red lines in Figure 5 will be used for the PA-12, PA-18, and PA-18 seaplane normal category airplanes with average wing loadings about 9.8 psf. The green lines will be used for the PA-12 and PA-18 utility category airplanes with average wing loading about 8.4 psf. The blue lines will be used for the PA-12 seaplane normal category airplane with average wing loading about 10.2 psf. The following data for the limit average maneuvering control surface loading, $K\bar{w}$, is taken from the graph in Figure 5 for curves A, B, and C at the various W/S conditions.

W/S	Curve A	Curve B	Curve C
~8.4 psf	19.5	17.0	13.5
~9.8 psf	22.5	19.5	15.5
~10.2 psf	23.5	20.5	16.0

Table 1 – Limit average maneuvering control surface loading

5.1 Maneuvering Rudder Loads CAM 3.219

CAM 3.219(a) was used to calculate the limit maneuvering rudder loads with the airplane in unaccelerated flight at zero yaw, a sudden displacement of the rudder control to maximum deflection as limited by the control stops or pilot effort, whichever is critical, shall be assumed.

The method in Figure 4 above (Fig 3-3(a)(3) from CAM 3) was used. For each of the airplane configurations listed, the value of $K\bar{w}$ was obtained from the graph at 20° rudder deflection for

the PA-12 (curve B) and 25° rudder deflection for the PA-18 (linear interpolation between curves A and B). The specific dimensions of three failed rudders (A, B, and C) were used for each of the airplane configurations to calculate the rudder post loads at the failure location. The calculations were not performed for Rudder D.

The average control surface loading at this condition was calculated using the following:

$$\overline{w} = K\overline{w}\frac{n}{4.4}$$

The total airload was then calculated for each airplane and rudder combination using:

$$w = \overline{w}A$$

Where A is the area of the rudder section that failed.

The maximum bending stress at the failure location was then calculated using the formula above. The calculation assumes a pristine material with nominal dimensions. Any corrosion, scratches, or other discrepancies in the rudder post would increase the maximum bending stress from the values calculated.

The calculated bending stress at the failure location showed that Rudder A had the largest bending stress for each condition due to its larger area and Rudder C had the smallest bending stress due to its smaller area. The bending stress varied from a low of 13.2 ksi for Rudder C on the PA-18 (normal) and PA-18S airplanes to a high of 18.1 ksi for Rudder A on the PA-18 (utility) airplane which are 24% and 33% of F_{tu}, respectively, for 1025 steel. In comparison these stress levels are 15% and 20% of F_{tu}, respectively, for 4130N steel.

CAM 3.219(b) was used to calculate the limit maneuvering rudder loads where the airplane shall be assumed to be yawed to a sideslip angle of 15° while the rudder control is maintained at full deflection (except as limited by pilot effort) in the direction tending to increase the sideslip.

The method in Figure 4 above (Fig 3-3(a)(4) from CAM 3) was used. For each of the airplane configurations listed, the value of $K\overline{w}$ was obtained from the graph using curve C. The specific dimensions of three failed rudders (A, B, and C) were used for each of the airplane configurations to calculate the rudder post loads at the failure location. The calculations were not performed for Rudder D.

The calculations used the same method as above to obtain the average control surface loading, total airload, and maximum bending stress at the failure location.

The calculated bending stress at the failure location showed that Rudder A had the largest bending stress for each condition due to its larger area and Rudder C had the smallest bending stress due to its smaller area. The calculated bending stress at the failure location varied from a low of 11.7 ksi for Rudder C on the PA-18 (normal) and PA-18S airplanes to a high of 13.7 ksi for Rudder A on the PA-12S airplane which are 21% and 25% of F_{tu}, respectively, for 1025 steel. In comparison these stress levels are 13% and 15% of F_{tu}, respectively, for 4130N steel.

CAM 3.219(c) was used to calculate the limit maneuvering rudder loads where the airplane shall be assumed to be yawed to a sideslip angle of 15° while the rudder control is maintained in the neutral position (except as limited by pilot effort). The assumed sideslip angles may be reduced if it is shown that the value chosen for a particular speed cannot be exceeded in the cases of steady slips, uncoordinated rolls from a steep bank, and sudden failure of the critical engine with delayed corrective action.

The method in Figure 4 above (Fig 3-3(a)(5) from CAM 3) was used. For each of the airplane configurations listed above, the value of $K\overline{w}$ was obtained from the graph using curve A. The specific dimensions of three failed rudders (A, B, and C) were used for each of the airplane configurations to calculate the rudder post loads at the failure location. The calculations were not performed for Rudder D.

The calculations used the same method as above to obtain the average control surface loading, total airload, and maximum bending stress at the failure location.

The calculated bending stress at the failure location showed that Rudder A had the largest bending stress for each condition due to its larger area and Rudder C had the smallest bending stress due to its smaller area. The calculated bending stress at the failure location varied from a low of 17.0 ksi for Rudder C on all airplanes except the PA-12S airplanes to a high of 20.1 ksi for Rudder A on the PA-12S airplane which are 31% and 36% of F_{tu}, respectively, for 1025 steel. In comparison these stress levels are 19% and 22% of F_{tu}, respectively, for 4130N steel.

5.2 Gust Rudder Loads CAM 3.220

CAM 3.220 was used to calculate the gust loads where the airplane shall be assumed to encounter a gust of 30 feet per second nominal intensity normal to the plane of symmetry while in unaccelerated flight at V_C, and the gust loads shall be calculated using the following formula:

$$\overline{w} = \frac{KUVm}{575}$$

Where:

$\overline{w}$ = average limit unit pressure in psf
U = nominal gust intensity in fps
V = airplane speed in mph
m = slope of lift curve of vertical surface C_L per radian
W = design weight in lb
S_V = vertical surface area in ft^2

$$K = 1.33 - \frac{4.5}{(W/S_V)^{3/4}}$$

A value of 2.51 for the lift curve slope was obtained from the FAA. The average limit gust loading on the various rudder segments was calculated for all the airplane configurations using the formulas above. The total airload due to gust was then calculated. The maximum bending

stress at the failure location was calculated using the formula above.

The calculated bending stress at the failure location showed that Rudder A had the largest bending stress for each condition due to its larger area and Rudder C had the smallest bending stress due to its smaller area. The calculated bending stress at the failure location varied from a low of 16.3 ksi for Rudder C on the PA-12 (utility) airplane to a high of 20.4 ksi for Rudder A on the PA-18 (normal) airplane which are 30% and 37% of F_{tu}, respectively, for 1025 steel. In comparison these stress levels are 18% and 23% of F_{tu}, respectively, for 4130N steel.

A summary table of all the calculated bending stresses is shown below. Examination of the results shows that the highest bending stresses in the rudder post were produced by the CAR 3.220 gust condition for the PA-18, normal and utility categories, with the CAR 3.219(c) maneuvering condition producing slightly lower stresses in those airplanes. For all PA-12 airplanes and the PA-18S airplane, the CAR 3.219(c) maneuvering condition produces the highest bending stresses in the rudder post with the CAR 3.220 gust loads producing slightly lower stresses. There was no scatter factor applied to the calculated loads which would result in much higher stresses. The detailed calculations for all the maneuvering and gust loads are shown in Appendix B.

Limit Bending Stress in Rudder Post for Maneuvering and Gust					
	Rudder	CAR 3.219(a) (ksi)	CAR3.219(b) (ksi)	CAR 3.219(c) (ksi)	CAR 3.220 (ksi)
PA-12 (normal)	A	16.7	13.3	19.3	18.6
	B	15.7	13.0	18.1	17.5
	C	14.7	12.6	17.0	16.4
PA-12 (utility)	A	16.9	13.4	19.3	18.5
	B	15.8	12.6	18.2	17.4
	C	14.9	11.8	17.0	16.3
PA-12S (normal)	A	17.6	13.7	20.1	18.6
	B	16.5	12.9	18.9	17.5
	C	15.5	12.1	17.7	16.4
PA-18 (normal)	A	15.0	13.3	19.3	20.4
	B	14.1	12.5	18.1	19.2
	C	13.2	11.7	17.0	18.0
PA-18 (utility)	A	18.1	13.4	19.3	20.4
	B	17.0	12.6	18.2	19.2
	C	16.0	11.8	17.0	18.0
PA-18S (normal)	A	15.0	13.3	19.3	18.6
	B	14.1	12.5	18.1	17.5
	C	13.2	11.7	17.0	16.4

Table 2 – Bending Stress for Maneuvering and Gust

6.0 Effect of Corrosion and Scratches

All 4 failed rudders examined had evidence of corrosion on the exterior surface of the rudder

post in the vicinity of the fractures. Rudder A had visible pitting in the vicinity of the fracture and Rudder C had a scratch associated with the fracture location. The pitting or scratching will act to increase the localized stress due to the loss of cross-sectional area and due to the stress concentration at the pit or scratch tip. Additionally, rudders A, B and C had faceted features and surface roughness consistent with being grit blasted. The angular features would also tend to locally increase the stress in the rudder post. The stress concentration factor, K_t, affects the nominal stress according to the following.

$$\sigma_{max} = K_t \sigma_{nom}$$

Which can be rearranged to:

$$K_t = \frac{\sigma_{max}}{\sigma_{nom}}$$

Utilizing the estimate above for the endurance limit of steel (0.50 of the tensile strength) we can examine the required stress concentration factor needed to increase the minimum and maximum calculated bending stresses due to maneuvering and gust to the point where they equal the endurance limits.

Required K_t	Estimated Endurance Limit (50% of F_{tu})	
	1025	4130N
Bending Stress	27.5 ksi	45 ksi
11.7 ksi	2.35	3.85
20.4 ksi	1.32	2.21

Table 3 – Required Stress Concentration

This shows that 4130 steel has a required K_t 0.9 to 1.5 higher than 1025 steel providing more margin.

Data for stress concentration factors is published in *Peterson's Stress Concentration Factors, Second Edition.* There is no data for a thin-walled tube in bending with a spherical notch or scratch. The US Air Force Life Cycle Management Center A-10 Structures and Aero Section performed a study for the NTSB to examine the stress concentration factor due to a spherical pit in a thin-walled tube in bending like the rudder post. The study examined pit diameters of 0.018-inch and 0.035-inch with depths from 0 to 0.035-inch (the wall thickness of the tube). The graph in Figure 6 below shows the results of the study. The study is presented in Appendix C.

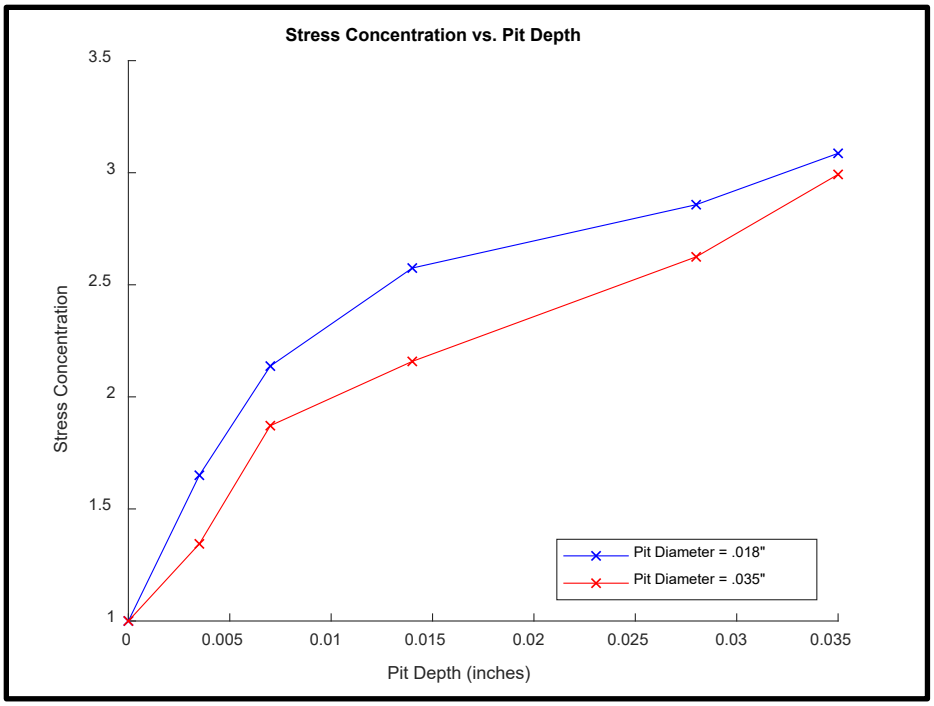

Figure 6 – Stress Concentration due to corrosion pit.

The results show an initial steep increase in the stress concentration up to a depth about 0.007-inch followed by a more gradual increase up to the tube wall thickness where the stress concentration approaches 3. A stress concentration of 3 agrees with data published in *Peterson's* for a hole in a thin infinite plate in bending. The stress concentration for the smaller diameter pit is higher throughout as expected. At the pit depth of 0.007-inch the stress concentration for the 0.018-inch diameter pit is 2.137 and for the 0.035-inch diameter pit is 1.871.

7.0 Effect of Strobe Light

The original drawing for the rudder had provisions for a strobe or beacon light at the top of the rudder post. All of the rudders examined were equipped with a light at the top of the rudder post though the exact details of each are unknown. The addition of a light to the top of the rudder post adds additional mass and surface area to the rudder. For the airload calculations the increased area would result in a small increase in the airload for each calculation that would increase the bending stress. The additional mass of the strobe would have an effect on the dynamic loads produced at the rudder post failure locations causing a further increase in the bending stress at the failure locations due to the forced vibrations of the upper rudder post. The vibratory response of the rudder could be affected by the blade pass frequency of the propeller, any propeller imbalance transmitted through the airframe, or even gust loading on the rudder.

The rudder post with strobe light is essentially a cantilevered beam with a concentrated mass at the top. The natural frequency is given by

$$\omega = \sqrt{\frac{k}{m}} = \sqrt{\frac{3EIg}{WL^3 + \frac{33}{140}wL^4}}$$

Where

E = 29,000,000 psi (modulus of elasticity)
I = 8.161 x 10^{-3} in^4 (moment of inertia)
g = 386.4 in/s^2 (gravitational acceleration)
W = 0.65 lb (weight of strobe)
L = 17.5625 in (length of rudder Post)
w = .09236 lb/in (distributed weight of post)

$$\omega = \sqrt{\frac{3(29{,}000{,}000)(8.161x10^{-3})(386.4)}{(.65)(17.5625)^3 + \frac{33}{140}(.09236)(17.5625)^4}} = 134.2\ \frac{rad}{s}$$

$$f = \frac{\omega}{2\pi} = \frac{134.2}{2\pi} = 21.4\ Hz$$

To examine the propeller blade pass frequency, we will assume a nominal engine speed of 2500 rpm with a 2-blade propeller resulting in a blade pass of 5000 per minute or 83.3 Hz. This is about 4 times the natural frequency of the rudder post with strobe light. In order to excite the rudder post at its natural frequency of 21.4 Hz the blade pass frequency would have to be about 1284 per minute which corresponds to an engine speed of 624 rpm.

The propeller blade pass frequency would equal the natural frequency of the rudder post only during a very brief time during start up and shut down. This brief excitation would not be expected to have a significant effect on the bending stress in the rudder post. It is possible that gust or other airframe vibrations could excite the natural frequency of the rudder post.

8.0 FAA Advisory Circular

The FAA published Advisory Circular (AC) 23-27 Parts and Materials Substitution for Vintage Aircraft in May 2009. The AC provides guidance for parts and material substitutions for old or out-of-production general aviation aircraft such as the Piper Super Cruiser or Super Cub where parts or material are difficult or impossible to obtain. The AC devotes the entire Appendix 2 to the material substitution of AISI 4130 steel for AISI 1020 or 1025 steel.

The AC states "You may substitute AISI (or other industry standard) 4130 low alloy steel in place of original AISI (or other industry standard) 1020 and 1025 plain carbon (non-sulfurized) steel" noting that "AISI 4130 is more readily available and has more desirable material properties than AISI 1020 and 1025-carbon steel." The AC further clarifies that the substitute material should have the same gage and wall thickness as the original, specifically noting that the 4130 has higher tensile ultimate strength, yield strength and fatigue strength than 1025, in general.

The FAA concludes "For structural tube on applicable aircraft, we permit the substitution of AISI 4130 steel (normalized) for either AISI 1020 or 1025 steel tube."

9.0 Conclusions

1. The material properties of AISI 1025 and AISI 4130 steel show that AISI 4130 has, in some cases, somewhat better corrosion resistance.
2. The ultimate tensile strength and endurance limit of AISI 4130 steel is 64% higher than AISI 1025 steel.
3. The tensile yield strength of AISI 4130 steel is 94% higher than AISI 1025 steel.
4. The calculated bending stress in the rudder post due to the certification maneuvering loads are 28% of F_{tu} on average for 1025 steel and 17% of F_{tu} on average for 4130N steel representing a 50% increase in the margin of safety for 4130N steel with respect to the endurance limit.
5. The calculated bending stress in the rudder post due to the certification gust loads are 33% of F_{tu} on average for 1025 steel and 20% of F_{tu} on average for 4130N steel representing a 76% increase in the margin of safety for 4130N steel with respect to the endurance limit.
6. The effect of a stress concentration due to a corrosion pit is more critical for 1025 steel increasing the bending stress in the rudder post above the endurance limit for much smaller pit sizes.
7. The propeller blade pass frequency is significantly higher than the natural frequency of the upper rudder post.